Results in Physics 13 (2019) 102336

Contents lists available at ScienceDirect

Results in Physics

journal homepage: www.elsevier.com/locate/rinp

Kinetic Monte Carlo simulation of sintering behavior of additively manufactured stainless steel powder particles using reconstructed microstructures from synchrotron X-ray microtomography

Yi Zhang[a], Xianghui Xiao[b,c], Jing Zhang[a,*]

[a] Department of Mechanical and Energy Engineering, Indiana University-Purdue University Indianapolis, Indianapolis, IN 46202, USA
[b] X-ray Science Division, Argonne National Laboratory, Lemont, IL 60439, USA
[c] NSLS-II Beamline, Brookhaven National Laboratory, 98 Rochester St, Upton, NY 11973, USA

ARTICLE INFO

Keywords:
Sintering
Simulation
Powder

ABSTRACT

In this study, the sintering behavior of additively manufactured stainless steel powder particles is simulated using a three-dimensional kinetic Monte Carlo (kMC) model. The initial microstructure of powder particles is reconstructed using micro-CT images from the Argonne National Laboratory's synchrotron X-ray micro-tomography facility. Using the model, the sintering characteristics of the powder, including its relative density, neck growth, and grain coarsening, are quantitatively analyzed. Sintering temperature directly affects the rate of densification and grain growth and coarsening. Higher temperature results in faster densification and grain growth. Additionally, the relationship between grain coarsening and densification is analyzed. It is observed that when the relative density is below 0.70, the powder particles undergo densification; whereas when the relative density is higher than 0.70, grain coarsening is the main mechanism.

Introduction

Powder bed fusion (PBF) has been widely used to fabricate additive manufactured (AM) or 3D printed metallic components. In the PBF process, a moving laser or electron beam source is used to melt or sinter metal powders layer-by-layer to form a desired metallic component [1]. Sintering induced densification and volume shrinkage play an important role on mechanical strength and geometric accuracy in the AM parts, which is a long-lasting issue for AM industry.

It is difficult to directly observe the sintering process of metallic powder in experiments, due to complicated thermal condition produced by the fast-moving laser or electron beam, and the rapid heating and cooling process. Therefore, numerical models at different length scales have been developed to investigate the sintering phenomenon, and to predict the sintered microstructure. Molecular dynamics (MD) method investigates the mass transportation mechanisms of sintering at atomistic level [2–5], but the atomistic model can only simulate nano-sized systems for a few nanoseconds. Discrete element model (DEM) can handle a system with thousands of particles, since it simplifies each particle as a single point [6,7]. However, this method is not suitable for high relative density systems, due to its neck size simplification. Continuum level models, including finite element (FE) model [8,9] and phase field model [10,11], calculate the sintering densification and mass transportation by solving the diffusion equations. However, these models need to solve the coupled densification and mass transport partial different equations, which do not illustrate the sintering mechanisms at atomistic scale.

Kinetic Monte Carlo (kMC) is a mesoscale model that has the capability to overcome the difficulties for sintering models mentioned above. The kMC algorithm can be applied to a three-dimensional (3D) geometry without losing its geometric accuracy. The whole sintering process, from the initial low relative density stage to the final high relative density stage, can be effectively studied [12]. Additionally, kMC models can provide critical information about sintering, including the evolution of grain shape, grain size, and overall relative density [13]. Tikare et al. developed a kMC model to simulate the sintering of a copper powder assembly [14]. The configurational changes of the powder assembly and relative density evolution were compared against experimental images measured using synchrotron radiation technique. In another study, the effect of powder size distributions on sintering was investigated by Bjørk et al. using a kMC model [15]. The sintered microstructures with different configurations, including monosized, normal size distribution, and log-normal distribution, were compared. The kMC model for nickel powder sintering in solid oxide fuel cell was

* Corresponding author.
E-mail address: jz29@iupui.edu (J. Zhang).

https://doi.org/10.1016/j.rinp.2019.102336
Received 19 April 2019; Received in revised form 5 May 2019; Accepted 6 May 2019
Available online 09 May 2019

developed by Hara et al. [16]. In their model, the surface energy and grain boundary energy of nickel were taken into account, so that the model showed a more realistic sintering behavior of the nickel powder assembly. Although the above mentioned efforts, there is a gap in accurate description of the staring microstructure, which may affect the modeling results afterwards. Therefore the major innovation of the work is adoption of the microstructure coming directly from the image data reconstructed from Synchrotron X-ray microtomography.

Based on the above discussions, the kMC model of additively manufactured stainless steel powder with a realistic microstructure has not been reported. Additionally, the temperature effect on the powder sintering behavior is absent, which is crucial to understanding the thermal aspects in the PBF process. Therefore, this work aims to develop a new kMC sintering model for stainless steel powder used in PBF process.

The paper is arranged as follows. Section "Model description" provides the model details. The microstructure of stainless steel powder particles is reconstructed using Argonne National Laboratory's synchrotron X-ray microtomography facility, with a spatial resolution of 300 nm. Then the time-dependent kMC algorithm is utilized to simulate the sintering process. The evolutions of microstructures at varying sintering temperatures are analyzed. Using this model, the temperature effect on grain structure and volume shrinkage can be used for optimizing the PBF process.

Model description

Microstructure reconstruction of powder particles using synchrotron micro-CT

Two steps are used in this study: (1) generation of initial polycrystalline powder microstructures using reconstructed micro-CT images, using a special grain growth algorithm, and (2) isothermal sintering of the powder microstructures at varying temperatures. The purpose of the grain growth modeling is to generate the powder assembly of grains with different grain orientations. For the isothermal sintering simulation, three different sets of temperatures are considered, and the temperature effect on sintering behavior of powder particles will be analyzed. The details of the two steps are described below.

The initial microstructure of the powder particles for the kMC model was generated by reconstructing the 3D micro-CT tomography images from the synchrotron X-ray facility beamline 32-ID-C at Argonne National Laboratory. In this work, the EOS Stainless Steel PH1 powder [17], a 15-5 stainless steel, was used. The powder was placed into a glass tube sample holder with a diameter of 0.7 mm. Then the 3D microstructure of the powder particles was measured by X-ray synchrotron radiation. The measured images were reconstructed to a 3D cylindrical microstructure with a resolution of 300 nm. Further, a cube with a side length of 120 μm was cut from the cylinder for the kinetic Monte Carlo simulation.

In the kMC model, the simulation domain is discretized to sites, and the microstructure is represented by the state or an integer of each site. In this case, the cubic domain is divided by 100 sites at each edge, with each site length of 1.2 μm. A 3D grid with 100 sites each along x, y, and z-axis directions, or total 1,000,000 sites is formed. Then the microstructures from the reconstructed powder particles are imported to the grid by assigning the state of each site. Specifically, the stacks of micro CT images are processed to a binary format, which contains only integer 1 for particles and 0 for pores. The values of the binary images are assigned to the sites layer-by-layer, such that an initial binary 3D simulation domain is formed, with q = 1 for particle, and q = 0 for pores, where q is the state of each site. It is noted that the grain states of particles should not be the same, since the grain orientation of adjacent particles may be different.

Moreover, in order to capture the grain growth, and to keep tracking the configurational change of each particle, an identical state value needs to be assigned to each particle to represent its unique grain orientation. The extrapolation of grain state information to the kMC sites is conducted using the grain growth algorithm [14]. In this work, the pore sites keep unchanged (q = 0), integer values q from 1 to 1000 are randomly assigned to the particle sites (originally q = 1), therefore the particles are composed of small grains. During the grain growth simulation, the grain size increases until most of the particle contains only one grain orientation. Additional information of the grain growth model is given in Section "Material properties used in the models". The reconstructed powder microstructure and the corresponding kMC model after the grain growth are shown in Fig. 1.

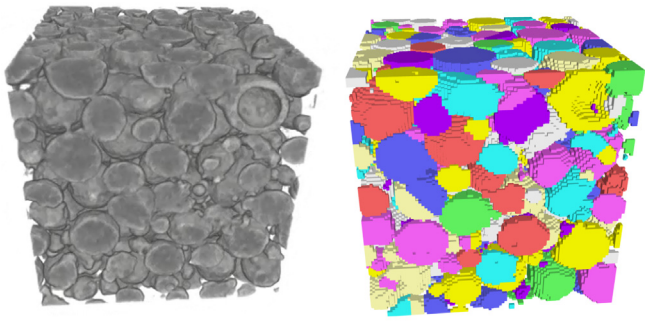

(a) (b)

Fig. 1. Microstructure of the 15-5 PH powder in a cubic domain with an edge length of 120 μm. (a) Micro CT reconstructed (resolution 300 nm), and (b) initial structure for the kMC model (resolution 1.2 μm). Colors in (b) denote grain crystal orientations.

Kinetic Monte Carlo sintering model

The kMC model is applied to the 3D microstructure to simulate the sintering of 15-5 PH1 powder particles during the PBF process. The kMC method has been previously used to simulate microstructure evolution during the solid-state sintering [14–16]. In the kMC model, sintering is realized by reducing the system's excessive energy. The excessive energy of a system E with a given microstructure is calculated by:

$$E = \frac{1}{2}\sum_{i=1}^{N}\sum_{j=1}^{n} J_{ij}(1 - \delta(q_i, q_j)) \tag{1}$$

where N is the total number of site; for each single site i, its excessive energy is the sum of energy of its n neighbor sites. For a 3D microstructure, the number of neighbors $n = 26$. The calculation of energy between sites i and j is based on the Kronecker delta function $\delta(q_i, q_j)$; if the state of sites i and j are the same ($q_i = q_j$), then $\delta = 1$; if $q_i \neq q_j$, then $\delta = 0$. Therefore, only the neighbors with different states will contribute to the excessive energy for the system. The term J_{ij} is a constant, which corresponds to the surface energy J_s if i and j are in pore-grain interaction, or the grain boundary energy J_{gb} if i and j are in grain-grain interaction. The value of surface energy, $J_s = 2.014 J/mol$, is taken from the *ab initio* calculation of iron [18], and the grain boundary energy, $J_{gb} = 1.115 J/mol$, is averaged from molecular dynamics calculation of 408 distinct grain boundaries of iron [19].

During sintering, the mechanisms include: (1) curvature driven grain growth, (2) surface diffusion induced pore reshaping and coarsing, and (3) densification and annihilation by the formation and diffusion of vacancies. During the densification and annihilation process, vacancies are generated from the grain boundary, and then they diffuse along grain boundaries until to the surface.

A standard Metropolis method is used for each step of the kMC simulation. The randomly selected site is attempted to migrate to its

neighbor, and then the system's excessive energy difference, ΔE, of the updated structure and previous structure is compared using Eq. (1). Next, the acceptance of the migration attempt is determined by probability P calculated by the following Eq. (2):

$$P = \begin{cases} 1, \ \&\Delta E < 0 \\ e^{\left(-\frac{\Delta E}{k_B T}\right)}, \ \&\Delta E \geq 0 \end{cases} \quad (2)$$

where k_B is the Boltzmann's constant and T is the temperature. If the excessive energy of the updated structure is lower than the previous step, $\Delta E < 0$, then the attempt of migration is accepted; if $\Delta E < 0$, then the acceptance of the attempt is determined by the term $e^{\left(-\frac{\Delta E}{k_B T}\right)}$. Instead of using the absolute temperature for T, the kMC model uses normalized $k_B T/J$ to represent the temperature. The scaling factor between the kMC temperature and real temperature can be determined by comparing the simulation results with experimental data [20]. Additionally, the kMC step is used to define the time in the simulation. Within each kMC step, every grain site ($q > 0$) makes one migration attempt. The kMC step in the simulation shows a linear relationship with actual time [21]. The ratio between kMCs and real time can also be determined by comparison and fitting the simulation results into experimental data.

Material properties used in the models

For microstructure reconstruction simulations in Section "Microstructure reconstruction of powder particles using synchrotron micro-CT" which involve grain growth only, we simulate the grain growth process, and the temperature for the pore migration and vacancy formation are set to 0. The temperature of the grain growth is $k_B T_{gg} = 1.0 J_{gg}$. To accelerate the simulation, a higher attempt frequency for grain growth, $f_{gg} = 20.0$, is employed. The simulation is stopped when most of the particles show a uniform grain orientation.

For the sintering simulation, the powder microstructure achieved from grain growth model in Section "Kinetic Monte Carlo sintering model" is imported as the initial configuration. Three different temperatures, T_0, $1.25T_0$ and $1.5T_0$, are simulated with 200,000 kMC steps. For the simulation of T_0, the temperature for grain growth is $k_B T_{gg} = 1.0 J_{gg}$, the temperature for pore migration is $k_B T_{pm} = 1.0 J_s$, and the temperature for vacancy formation is $k_B T_{vf} = 13.0 J_s$. The ratios between temperature parameters are defined to represent real sintering behavior of the powder particles, which are similar to other kMC metal powder sintering models [14,16]. The attempt frequencies are chosen in the ratio of 1:1:1 for grain growth, pore migration and vacancy formation, respectively. A list of temperature parameters for T_0, $1.25T_0$ and $1.5T_0$ is shown in Table 1, where the grain boundary energy $J_{gb} = 1.115 J/mol$, and surface energy $J_s = 2.014 J/mol$, and the ratios between each parameter are fixed.

All the simulations in this work are performed using SPPARKS kinetic Monte Carlo simulator package [22]. The material properties of stainless steel, surface and grain boundary energies, are incorporated into the model according to Hara et al. work [16]. Additional information of the model is available in our previous works [7,23–30]. In order to implement surface energy and grain boundary energy for stainless steel in the model, the source code for excessive energy calculation, J_{ij}, is modified.

Table 1
Temperature parameters for isothermal sintering at T_0, $1.25T_0$ and $1.5T_0$.

Temperature	$k_B T_{gg}/J_{gg}$	$k_B T_{pm}/J_s$	$k_B T_{vf}/J_s$
T_0	1.0	1.0	13.0
$1.25T_0$	1.25	1.25	16.25
$1.5T_0$	1.5	1.5	19.5

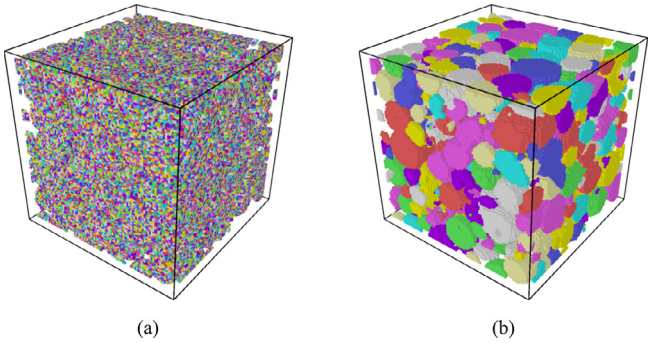

Fig. 2. Microstructure of 15-5PH1 powder particles in a $120 \times 120 \times 120\ \mu m^3$ cubic simulation domain, (a) before grain growth, and (b) after 1000 kMCs grain growth. Colors show the grain orientations. (For interpretation of the references to colour in this figure legend, the reader is referred to the web version of this article.)

Results and discussion

Initial microstructure using grain growth model

Fig. 2 shows the microstructure before (Fig. 2a) and after (Fig. 2b) the grain growth simulations. The initial microstructure shows a different grain orientations among each voxel. During the grain growth, grain size increases, and the total number of grain decreases. Since in this model, temperatures for pore migration and vacancy formation are set zero, therefore the shapes of particles and pores remain unchanged. The grains keep expanding till 1000 kMCs, where a stabilized grain microstructure is obtained. In the final configuration, most of the particles show a single uniform orientation. For a few particles with relatively large particle size, two or more orientations can be observed. Most of the adjacent particles are distinguishable with different orientations, which shows the capability for grain growth simulation. The microstructure achieved from the grain growth model is imported for sintering simulation.

Sintering simulation results

In the sintering simulation, the site values at different time are recorded for configuration analysis. The configurational changes of the 15-5PH1 powder during isothermal sintering at T_0 are shown in Fig. 3. The initial microstructure shows clearly distinct particles, most of the particles are nearly in spherical shape, and they are connected with little contact. As the sintering begins (Fig. 3b), the gaps between the particles are decreased, and the "neck" formation between particles can be observed. At the same time, the pore volume around the entire powder particles increases, which means the powder volume shrinkages toward the center of the model. The phenomenon, neck growth and slightly densification, clearly indicates that sintering undergoes initial stage at this moment. At the period between 20,000–80,000 kMCs, the powder particles' volume shrinkage and grain growth happen simultaneously. The powder particles' volume decreases and grain size increases obviously. This is consistent with characteristics of intermediate stage of sintering, where grain growth and densification dominate. At this instant (Fig. 3c), larger grains connect to each other, with closed pores inside the network. After the intermediate stage of sintering, as shown in Fig. 3d, compared to Fig. 3c, the relative density and grain size do not change a lot. However, some pores inside the structure are eliminated. This is because in the final stage of sintering, the grain growth and densification show a much slower rate, and the main phenomenon is the elimination of small pores and the growth of large pores.

By using the powder configurational change results in Fig. 3, the grain size evolutions are analyzed. In the simulation domain,

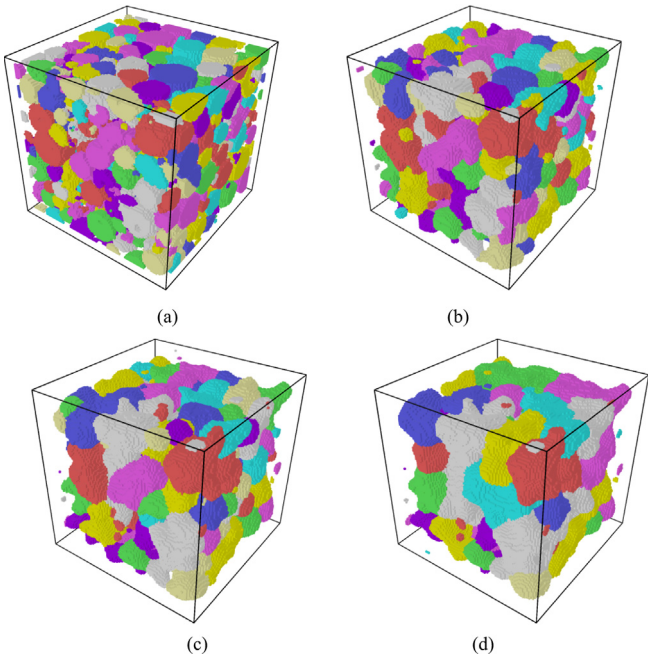

Fig. 3. Configurational changes of the 15-5 PH1 powder particles sintered at temperature T_0 ($k_B T_{gg} = 1.0 J_{gg}$, $k_B T_{pm} = 1.0 J_s$, $k_B T_{vf} = 13.0 J_s$). (a) 0 kMCs, (b) 20,000 kMCs, (c) 80,000 kMCs, and (d) 200,000 kMCs.

continuous sites with the same non-zero state are considered as the same grain. In order to remove the noise, i.e., small isolated sites at the domain boundaries, the grains with size less than 100 sites are ignored from grain size statistics. Grain size distributions before and after sintering are shown in Fig. 4. Specifically, the relative frequency and cumulative percentage at the end of the simulation are compared with the initial powder microstructure. Before sintering (0 kMCs), the powder sizes of the initial structure are distributed in a narrow range, 6–33 μm, and the mean particles size is about 15 μm. During the sintering process, the average grain size increases. At the end of the simulation (200,000 kMCs), grain sizes are distributed in a much wider range. And the mean grain size increases to about 24 μm.

Densification of particles sintered at varying temperatures is represented by the evolution of relative density shown in Fig. 5a. A similar trend of relative density evolution can be observed for all temperatures: the relative density suddenly increased from 0.58 to larger than 0.60 in a very short time. After that, the rate of densification decreases with time, until a very slow change at the end of simulation. This shows the characteristic of different sintering stages. In the initial and intermediate stages, the particles undergo neck growth, fast densification; whereas in the final stage, these mechanisms are much slower. With the same initial relative density, when sintered at temperatures T_0, $1.25T_0$ and $1.5T_0$, the final relative density increased to 0.751, 0.781 and 0.786, respectively. Higher density in the sintered product can be achieved by increasing the sintering temperature. The final configurations at each temperature are shown in Fig. 5b. The powder volume is slightly different, which is consistent with the relative density result. The overall shapes of the sintered powder particles are similar. Powder microstructures sintered at higher temperature show a larger grain size and fewer number of grain.

A more detailed analysis on temperature effect on grain growth with time is given in Fig. 6. As shown in Fig. 6a, there are nearly 400 distinct particles in the initial microstructure. During the sintering process, the number of grain drops to less than 300 only in a few steps as sintering begins (less than 10,000 kMCs). This indicates that at this period, particles are connected by neck formation and neck growth. During the time of 10,000–100,000 kMCs. The number of grain keeps decreasing very fast, and the average grain size increases (Fig. 6b). At this stage, the rapid grain growth is due to the merging of small particles into larger ones. When the time is longer than 100,000 kMCs, the number of grain decreases at a lower rate, and the average grain size keeps increasing at a lower rate. Since in the final stage of sintering, the system undergoes slow grain growth and densification.

Using the densification history and average grain size information from Figs. 5a and 6b, the grain size with respect to relative density is plotted in Fig. 7. The purpose of this figure is to illustrate the role of densification and grain coarsening at different stage of sintering. As shown in the figure, although the sintering temperatures are different, the relationship between the relative density and grain size basically remain the same. As the relative density increases, the grain size increases linearly from 0.58 to 0.70 with a relatively small slope, indicating that when the relative density is low (less than 0.70), the systems undergoes densification without rapidly grain growth. When the relative density is larger than 0.70, the grain size shows a linear increment with a larger slope. This means that when the relative density is large, the relative density does not change rapidly anymore. Instead, the major phenomenon that the system undergoes is grain growth and coarsening.

Conclusions

A new kMC model for additively manufactured 15-5 PH1 stainless

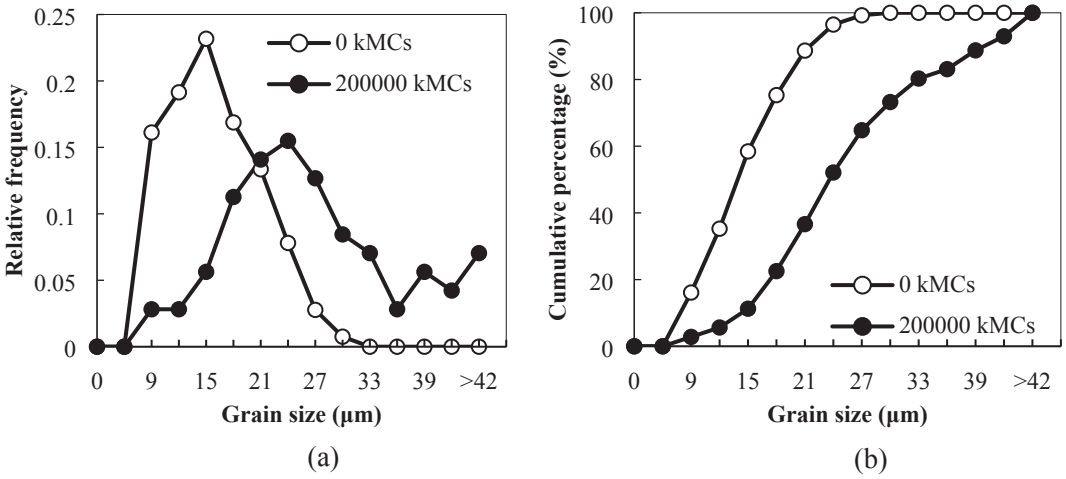

Fig. 4. Grain size distribution of 15-5 PH1 powder before sintering (0 kMCs) and after sintering (200,000 kMCs) at temperature T_0. (a) Relative frequency, (b) Cumulative percentage.

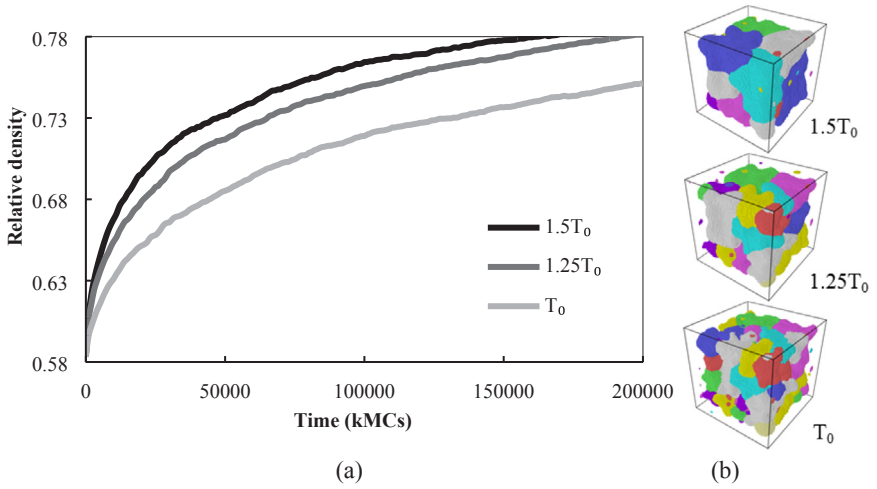

Fig. 5. (a) Relative density evaluation at varying temperatures, and (b) the final configurations at three different temperatures.

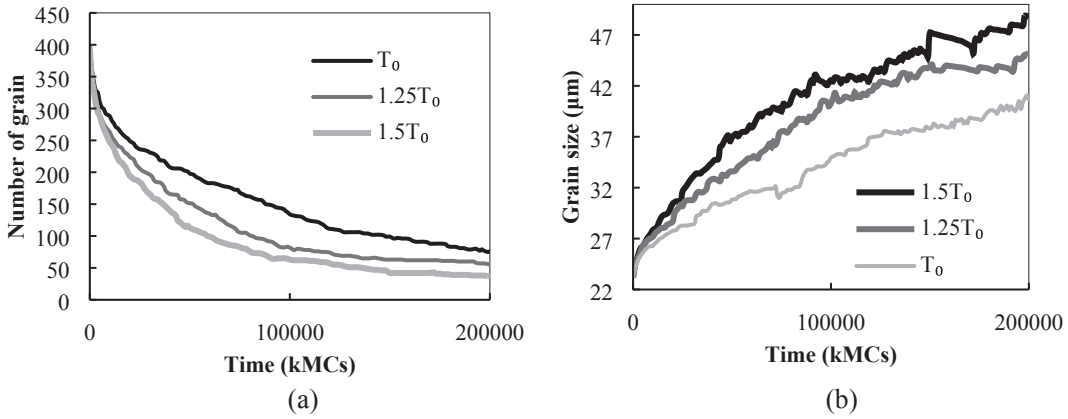

Fig. 6. Evolutions of grains in the sintered powder microstructure: (a) number of grains, and (b) average grain.

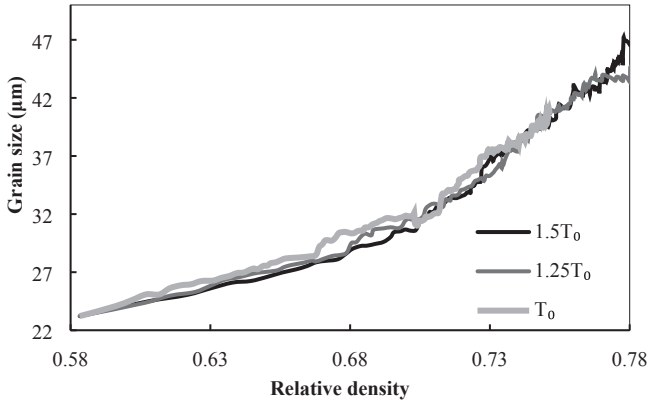

Fig. 7. Average grain size with respect to relative density.

steel powder particles is presented. In this model, the initial microstructure of the powder particles is achieved from the synchrotron micro-CT technique. Material specific properties, including surface energy and grain boundary energy, are taken into account into the model. In order to utilize the micro CT images for kMC sintering simulation, the grain growth simulation is conducted before the sintering to generate distinct particles with different grain orientations. The conclusions of the work are summarized as follows:

1) The kMC model has the capability to capture all three stages of sintering phenomena in additively manufactured powder particles, includes the neck formation in the initial stage, grain growth and densification in the intermediate stage, and the pore elimination in the final stage.
2) Sintering temperature directly affects the rate of densification and grain growth and coarsening. Higher temperature results in faster densification and grain growth. Also, with higher sintering temperature, the sintered powder particles show a higher relative density, larger grain size, and less number of grains.
3) The relationship between grain coarsening and densification is analyzed. It is observed that when the relative density is below 0.70, the powder particles undergo densification; whereas when the relative density is higher than 0.70, grain coarsening is the main mechanism.

Acknowledgements

The authors acknowledge the financial support provided by Walmart Foundation (project title: Optimal Plastic Injection Molding Tooling Design and Production through Advanced Additive Manufacturing) and Praxair Surface Technologies TruForm AMbition Grant. This research used resources of the Advanced Photon Source, a U.S. Department of Energy (DOE) Office of Science User Facility operated for the DOE Office of Science by Argonne National Laboratory under Contract No. DE-AC02-06CH11357. The micro-tomography data was collected at the X-ray Operations and Research beamline 32-ID-C at the Advanced Photon Source, Argonne National Laboratory.

Declaration of Competing Interest

The authors declare that they have no conflict of interest.

Appendix A. Supplementary data

Supplementary data to this article can be found online at https://doi.org/10.1016/j.rinp.2019.102336.

References

[1] Zhang Y, et al. Additive manufacturing of metallic materials: a review. J Mater Eng Perform 2017.
[2] Ding L, Davidchack RL, Pan J. A molecular dynamics study of sintering between nanoparticles. Comput Mater Sci 2009;45(2):247–56.
[3] Zhang Y, et al. Molecular dynamics simulation of electrical resistivity in sintering process of nanoparticle silver inks. Comput Mater Sci 2016;125:105–9.
[4] Zhang Y, et al. Molecular dynamics study of the strength of laser sintered iron nanoparticles. Proc Manuf 2015;1:296–307.
[5] Zhang Y, Zhang J. Sintering phenomena and mechanical strength of nickel based materials in direct metal laser sintering process—a molecular dynamics study. J Mater Res 2016;31(15):2233–43.
[6] Martin S, et al. Simulation of sintering using a non smooth discrete element method. Application to the study of rearrangement. Comput Mater Sci 2014;84:31–9.
[7] Lee W-H, Zhang Y, Zhang J. Discrete element modeling of powder flow and laser heating in direct metal laser sintering process. Powder Technol 2017;315:300–8.
[8] Mori K. Finite element simulation of powder forming and sintering. Comput Methods Appl Mech Eng 2006;195(48–49):6737–49.
[9] Kucherenko S, Pan J, Yeomans JA. A combined finite element and finite difference scheme for computer simulation of microstructure evolution and its application to pore-boundary separation during sintering. Comput Mater Sci 2000;18(1):76–92.
[10] Wang YU. Computer modeling and simulation of solid-state sintering: a phase field approach. Acta Mater 2006;54(4):953–61.
[11] Ahmed K, et al. Particle-grain boundary interactions: a phase field study. Comput Mater Sci 2017;134:25–37.
[12] Cardona CG, et al. On sintering stress in complex powder compacts. J Am Ceram Soc 2012;95(8):2372–82.
[13] German RM. Coarsening in sintering: grain shape distribution, grain size distribution, and grain growth kinetics in solid-pore systems. Crit Rev Solid State Mater Sci 2010;35(4):263–305.
[14] Tikare V, et al. Numerical simulation of microstructural evolution during sintering at the mesoscale in a 3D powder compact. Comput Mater Sci 2010;48(2):317–25.
[15] Bjørk R, et al. The effect of particle size distributions on the microstructural evolution during sintering. J Am Ceram Soc 2013;96(1):103–10.
[16] Hara S, Ohi A, Shikazono N. Sintering analysis of sub-micron-sized nickel powders: kinetic Monte Carlo simulation verified by FIB–SEM reconstruction. J Power Sources 2015;276:105–12.
[17] Shui A, Uchida N, Uematsu K. Origin of shrinkage anisotropy during sintering for uniaxially pressed alumina compacts. Powder Technol 2002;127(1):9–18.
[18] Schönecker S, et al. Thermal surface free energy and stress of iron. Sci Rep 2015;5:14860.
[19] Ratanaphan S, et al. Grain boundary energies in body-centered cubic metals. Acta Mater 2015;88:346–54.
[20] Zhang Y, Xia C, Ni M. Simulation of sintering kinetics and microstructure evolution of composite solid oxide fuel cells electrodes. Int J Hydrogen Energy 2012;37(4):3392–402.
[21] Limoge Y, Bocquet JL. Monte carlo simulation in diffusion studies: time scale problems. Acta Metall 1988;36(7):1717–22.
[22] SandiaNationalLaboratories. Crossing the mesoscale no-man's land via parallel kinetic Monte Carlo. United States Department of Energy; 2009.
[23] Sagar S, et al. Room-temperature charpy impact property of 3d-printed 15–5 stainless steel. J Mater Eng Perform 2018;27(1):52–6.
[24] Zhang J, et al. Comparison of virgin and reused 15–5 PH stainless steel powders for laser powder bed fusion process. Prog Additive Manuf 2018(1–2).
[25] Zhang J, Jung Y-G, editors. Additive manufacturing: materials, processes, quantifications and applications. 1st ed.Elsevier; 2018. p. 362.
[26] Zhang J, et al. A multi-scale multi-physics modeling framework of laser powder bed fusion additive manufacturing process. Met Powder Rep 2018;73(3):151–7.
[27] Zhang Y, et al. Additive manufacturing processes and equipment. Addit Manuf 2018:39–51.
[28] Zhang Y, et al. Multiscale multiphysics modeling of laser powder bed fusion process. Additive manufacturing. Elsevier; 2018. p. 215–59.
[29] Zhang Y, et al. Temperature-dependent charpy impact property of 3D printed 15-5 stainless steel. Materials science and technology 2018 (MS&T18), October 14–18, 2018, Greater Columbus Convention Center, Columbus, Ohio, USA. 2018.
[30] Zhang Y, Zhang J. Finite element simulation and experimental validation of distortion and cracking failure phenomena in direct metal laser sintering fabricated component. Addit Manuf 2017;16:49–57.